Journal of Materials Chemistry A

Accepted Manuscript

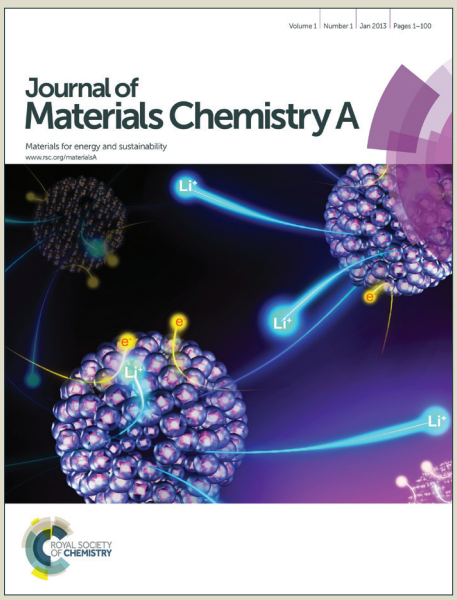

This is an *Accepted Manuscript*, which has been through the Royal Society of Chemistry peer review process and has been accepted for publication.

Accepted Manuscripts are published online shortly after acceptance, before technical editing, formatting and proof reading. Using this free service, authors can make their results available to the community, in citable form, before we publish the edited article. We will replace this *Accepted Manuscript* with the edited and formatted *Advance Article* as soon as it is available.

You can find more information about *Accepted Manuscripts* in the Information for Authors.

Please note that technical editing may introduce minor changes to the text and/or graphics, which may alter content. The journal's standard Terms & Conditions and the Ethical guidelines still apply. In no event shall the Royal Society of Chemistry be held responsible for any errors or omissions in this *Accepted Manuscript* or any consequences arising from the use of any information it contains.

ROYAL SOCIETY OF CHEMISTRY

www.rsc.org/materialsA

Journal Name

RSCPublishing

ARTICLE

A solar-driven photocatalytic fuel cell with dual photoelectrode for simultaneous wastewater treatment and hydrogen production

Cite this: DOI: 10.1039/x0xx00000x

Received ooth xx 20xx,
Accepted ooth xx 20xx

DOI: 10.1039/x0xx00000x

www.rsc.org/

Zhongyi Wu, Guohua Zhao,* Yajun Zhang, Jian Liu, Ya-nan Zhang and Huijie Shi

A solar-driven dual photoelectrode photocatalytic fuel cell (PFC) based on n-type semiconductor photoanode and p-type semiconductor photocathode is reported for wastewater treatment with simultaneous hydrogen production. The PFC shows a superior performance of phenol degradation and hydrogen production with a maximum TOC removal rate of 84.2 % and a total hydrogen producing rate of 86.8 μmol cm^{-2} in 8 hours which is much higher than other similar researches. Compared to the system comprised of a photoanode (photocathode) and Pt for phenol degradation (hydrogen production), the results proves that there is a synergistic effect between the two photoelectrodes. Because the electrons store on the photocathode for hydrogen production and holes on the photoanode for pollutants degradation preferably. Several semiconductors are chosen as photoelectrode to investigate the factors influencing the performance of PFC system. The V_{OC} value of PFC increases with the difference of Fermi level between the two photoelectrodes. This PFC system provides a new approach for efficient energy recovery from the wastewater.

Introduction

Energy and environment quality are two major issues faced by countries in modern society.[1,2] Simultaneous wastewater treatment and energy recovery by solar energy conversion is an attractive and promising technology. As a result of the rapid development of the industrialization, the environmental pollution, especially the water pollution, becomes more and more serious due to the rapid increasing effluent discharge. As we know, pollutants degradation is the main purpose of traditional wastewater treatment method, but the huge amount of chemical energy are ignored at the same time.[3] It is urgent for us to seek new and efficient methods for wastewater treatment to eliminate pollution and obtain energy.

Microbial Fuel Cell (MFC) realizes the concept, which can generate electricity during the degradation of organic matters by microbial community.[4-6] The MFC converts the energy of organic pollutants presented in wastewater into electric current. However, because of the relatively low current efficiency, researchers switch to produce hydrogen with the MFC combined with electrocatalysis or photocatalysis.[7,8] As is known, hydrogen is a kind of green energy because of no secondary pollution. However, MFC is not feasible to treat some persistent organics due to their biorefractory nature. The harsh working condition, slow electron transfer and complicated bacteria cultivation also obstruct the large-scale commercial application of MFC.

As we know, light is a kind of cost-free, clean and convenient energy. So the idea that we use light as a substitute for microorganism has come to the fore. So a novel photoelectrocatalytic (PEC) system for hydrogen production has been proposed. Previously, many researchers focus on hydrogen production by the PEC water reduction on a single photocatalyst.[9,10] A highly active $Cu_2O/(ZnO/Al_2O_3)/TiO_2/Pt$ photocathode is used for water reduction.[11] A CdS-cluster-decorated graphene nanosheets is applied for highly efficient visible-light-driven photocatalytic hydrogen production.[12] Then, a two-electrode PEC system composed by $Cu/nanoCu_2O/NiO_X$ photocathode and the $FTO/nanoWO_3$ photoanode is used for PEC hydrogen production.[13] However, the PEC system for hydrogen production needs external electric energy input. The cost is and energy consumption are both high. As a result, it is insufficient from the point of view of energy recovery.

Journal of Materials Chemistry A Accepted Manuscript

At the same time, the PEC system is used for organic wastes degradation.[14] Then a solar-driven biomass fuel cell is used for electricity generation from the wastewater.[15] A single photoelectrode photocatalytic fuel cell (PFC) under light illumination is applied for refractory organic pollutants degradation and simultaneous electricity generation.[16-18] A visible light driven PFC composed of BiOCl/Ti photoanode and Pt cathode is used for organic pollutants degradation and electricity generation.[19] Then the dual photoelectrode of WO_3/W or TiO_2/Ti as photoanode and Cu_2O/Cu as photocathode under visible light illumination is applied for simultaneous wastewater treatment and electricity generation.[20,21] In conclusion, these works focus on the degradation of pollutants on the photoanode and the electricity generation performance. However, there are so many factors affecting the performance of PFC. No further research about specific mechanism of PFC is discussed. So it is meaningful to discover a theoretical guidance for the selection of photoelectrodes in the PFC. Meanwhile, the PFC cannot only be used for simultaneous wastewater treatment in anode area and energy recovery, but it is also considered that specific attention should be paid to the cathode reaction.

Therefore, a solar-driven dual photoelectrode PFC for simultaneous organic pollutants degradation and hydrogen production has come to the fore. This approach combined the advantages of the two system mentioned above. As we know, the electrons and holes of semiconductor will be separated under light illumination and there will be a photovlotage. For the n-type semiconductor under the light illumination photo-generated holes is the majority for oxidation. In contrast, for the p-type semiconductor under the light illumination the photo-generated electrons is the majority for reduction.[22,23] So we consider whether the photovoltage difference between two different semiconductors can be used for the pollutant oxidation on photoanode and simultaneous hydrogen production on photocathode. If possible, the photoanode of the PFC should be an n-type semiconductor and has a good photocatalytic property for the pollutant oxidation such as TiO_2, CdS and so on.[24-30] The photocathode of the PFC should be a p-type semiconductor whose E_{CB} (VS. NHE) should be more negative than $E_{H+/H2}$ of 0 V due to the purpose of hydrogen production, such as Cu_2O.[31-34]

To investigate simultaneous pollutants treatment and hydrogen production, a sealed quartz reactor is used for hydrogen collection which is shown in Fig. S1. Phenol was selected as the representative organic pollutant to study the degradation performance of PFC.[35, 36]

Furthermore, the most important thing for the PFC is the operation mechanism. So for the study of the operation mechanism of PFC, several n-type and p-type semiconductors have been chosen to verify the feasibility of the target. Here, n-TiO_2, n-CdS, n-CdSe and p-Cu_2O have been chosen as the photoelectrode. What's more, the same semiconductor with different microstructure has also been chosen. This work provides an effective and low energy consumptive approach for simultaneous environmental pollutant disposal and energy recovery by using photocatalyic system.

Experimental Section

Electrodes preparation

Photoanode. TiO_2 NRs/FTO: The titanium butoxide (0.35mL) (Aladdin, AR, 99.0%) was dropwise added into a HCl (SCRC,AR, 36.0-38.0%) aqueous solution (6mol L^{-1}, 15mL) under continuous stirring for 30 min at room temperature. Then the solution was transferred to a Teflon-lined stainless steel autoclave, and a piece of FTO sample was immersed in the solution with the conductive surface facing down. The autoclave was sealed and placed in an oven at 150℃ for 4h with the heating and cooling rates of 5℃min^{-1}. After cooling the autoclave to the room temperature, the TiO_2 NRs/FTO was rinsed several times with deionized water and dried in the air.[37] The SEM image of TiO_2 NRs/FTO is shown in Fig. S2A.

TiO_2 NTs/Ti: Firstly, TiO_2 NTs were prepared by a two-step electrochemical anodic oxidation method according to the literature. After that, it was annealed in air atmosphere for 3h with the heating and cooling rates of 5℃min^{-1}. The detailed preparation procedure is shown is ESI. [38]

CdSe NPs/FTO: The applied potential of electrodeposition was -1.1V vs SCE and the deposition time was 2 h. Then the CdSe NPs/FTO were rinsed thoroughly and annealed at 300 °C in N_2 atmosphere for 3 h by the tube furnace (SOM, SGL-1200Z). The detailed preparation procedure is shown is ESI.[39]

CdS NPs/FTO: The applied potential of electrodepositon was -0.65 V vs SCE and the deposition time was 1000 s. The thermostatted bath temperature was 70 ℃ . Then the CdS NPs/FTO were rinsed and annealed at 500 °C in N_2 atmosphere for 6 h. The detailed preparation procedure is shown is ESI.[40]

Photocathode. C/Cu NWAs/Cu mesh: The Cu mesh (Alfa Aesar, 100 mesh, 0.11 mm as wire diameter) was anodized in an NaOH (Aladdin, AR, 96.0%) solution (3 mol L^{-1}) for 20 min under 10 mA cm^{-2} to form $Cu(OH)_2$ NWAs/Cu mesh at 25 °C. The $Cu(OH)_2$ NWAs/Cu mesh was inmmersed into 3 mg mL^{-1} glucose solution which was prepared using deionized water for glucose coating. Then the $Cu(OH)_2$ NWAs/Cu mesh with glucose coating was annealed at 550 °C at N_2 atmosphere for 4 h with the heating and cooling rates of 5℃min^{-1}.[41] The SEM images of Cu NWAs/Cu mesh with or without carbon layer are shown in Fig. S2B and C.

Cu_2O NPs/FTO: The electrochemical deposition was performed potentiostatically with a potential of −0.3 V (versus Ag/AgCl) for 30 min and the temperature of the electrolyte was kept at 60℃ by water bath. The detailed preparation procedure is shown is ESI.[42]

Characterization methods

The morphology of the sample photoelectrodes were identified by using a field emission scanning electron microscopy (FE-SEM, Hitachi S-4800, Japan). Detailed microstructural features of the sample electrodes were investigated by high resolution

Journal of Materials Chemistry A Accepted Manuscript

 This journal is © The Royal Society of Chemistry 2014

transmission electron microscopy (HR-TEM, JEM2100, JEOL, Japan), using a JEM-2000EX electron microscope operated at 200 kV. The crystalline structure of the samples were analysed by X-ray diffraction (XRD, D8 Focus X-ray diffractometer, Bruker, Germany), using Cu Kαradiation (λ= 1.540598 Å). The UV-vis diffuse reflectance absorption spectra (UV-vis DRS) were recorded by AvalightDHS UV-Vis absorbance measurements (Avantes, Netherlands).

Photoelectrochemical measurement

The photoelectorchemical Characterizations of the photoelectrodes were carried out by using a three-electrode configuration with the samples, platinum foil and $Ag/AgCl_2$, as working electrode, counter electrode and reference electrode, respectively. The working electrode parameters were controlled by an electrochemical workstation (CHI660C, USA). The photocatalytic fuel cell (PFC) was set up using two electrode configurations. The photoanode and photocathode were immersed in the solution in a quartz reactor and illuminated with one light source. Herein, a 300 W PSL-SXF300 Xe lamp (Changtuo, China) was used as simulated solar light source, without further description, all experiments were carried out under AM 1.5 (light intensity, 100 mW cm^{-2}) solar light irradiation by using a AM 1.5 filter which supplied by PerfectLight (Beijing, China). All the experiments were carried out in a rectangular quartz reactor (V=435mL) with the working area of the photoanode and photocathode of both $2cm^2$, moderate stirring, without applying external potential (see fig. S1 in ESI). Linear sweep voltammetry was used to obtain the I-V characteristics curves in one typical cycle at a scan rate of 0.02 V s^{-1}.[20] The I-V characteristics curves of the PFCs were measured in a two electrode system, where the anode served as the working electrode and the cathode as the counter and reference electrodes. The voltage and power were obtained as a function of current density, and normalized to the photocathode area. The power density (P) was calculated from $P = I \times V$.

The organic compounds degradation was carried out in a quartz reactor under AM 1.5 (light intensity, 100 mW cm^{-2}) solar light irradiation, too. The target organic compound was phenol (20 mg L^{-1}) and 0.1 mol L^{-1} Na_2SO_4 was used as the electrolyte. The TOC removal rate of phenol was monitored by TOC (multi N/C 3100 TOC/TN_b analyzer, Analytikjena, Germany).

The total hydrogen amount produced was calculated by multiplying the hydrogen content in a 1 mL gas sample with the headspace volume of the PFC reactor (200 mL).[43] The hydrogen was measured by gas-chromatography (GC 7900, Techcomp, Shanghai, China).

Results and Discussion

PEC performance, TOC removal and Hydrogen production of PFC

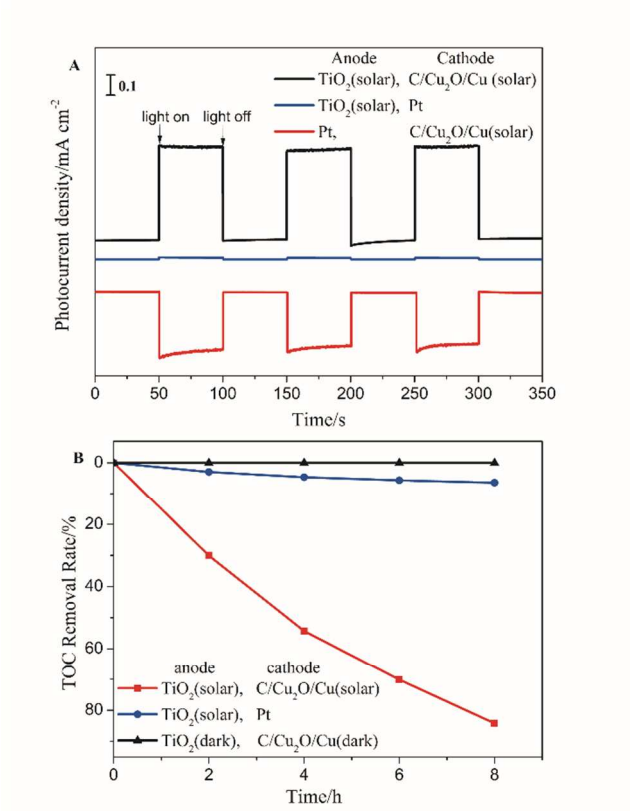

Fig. 1 A: the photocurrent of TiO_2 NRs/FTO, C/Cu_2O NWAs/Cu and PFC system, where the substrate is 0.05 mol L^{-1} phenol and support electrolyte is 0.1 mol L^{-1} Na_2SO_4 under AM 1.5 illumination (light density, 100 mW cm^{-2}), and the area of photoelectrodes are both 2 cm^2; B: the TOC removal rates of phenol (20mg L^{-1}) TiO_2 NRs -Pt and TiO_2 NRs, C/Cu_2O NWAs/Cu PFC under light ililumination and in dark.

Fig. 1A presents the photocurrent of TiO_2 NRs/FTO, C/Cu_2O NWAs/Cu, and TiO_2 NRs/FTO - C/Cu_2O NWAs/Cu PFC, respectively. The SEM and UV-Vis absorption of them are show in Fig. S2 and Fig. S3. And there is almost no photoresponse for the TiO_2 NRs/FTO photoanode. It may be because TiO_2 is a broadband semiconductor and it only has a response to ultraviolet light (UV-light). However, the light source we used is the solar light source in which the UV-light only has a percentage of about 5%. So under the solar light illumination, there is almost no photoresponse for the TiO_2 NRs/FTO photoanode. Because Cu_2O is a narrowband semiconductor which has a response to the visible light and there is a large proportion of visible light in

Journal of Materials Chemistry A Accepted Manuscript

Journal Name RSCPublishing

ARTICLE

Table 1. The photocurrent density of photoelectrodes and PFCs.

PFC No.[a]	Photoanode	Photocathode	J_1[c] (mA cm^{-2})	J_2[d] (mA cm^{-2})	J_{SC}[e] (mA cm^{-2})	$J_{SC}'=J_1+J_2$ (mA cm^{-2})
C1	**TiO_2 NRs[b]**	**C/Cu_2O/Cu**	0.01	0.41	0.50	0.42
C2	**TiO_2 NRs**	**Cu_2O**	0.01	0.25	0.33	0.26
C3	**TiO_2 NTs/Ti**	**C/Cu_2O/Cu**	0.005	0.41	0.25	0.415
C4	**TiO_2 NTs/Ti**	**Cu_2O**	0.005	0.25	0.20	0.255
C5	**CdS**	**C/Cu_2O /Cu**	0.30	0.41	0.61	0.71
C6	**CdS**	**Cu_2O**	0.30	0.25	0.31	0.55
C7	**CdSe**	**C/Cu_2O/Cu**	0.10	0.41	0.16	0.51
C8	**CdSe**	**Cu_2O**	0.10	0.25	0.11	0.35

a, the number of PFC is applicable to the following Figures and Tables.

b, the substrate of material without noted is FTO, and this is also applicable to the following tables.

c & d, J_1 and J_2 are the photocurrent density of photoanode and photocathode, respectively.

e, J_{SC} is measured in the initial 10 minutes while the PFC is working, and this is also applicable to the following tables.

the solar light, the C/Cu_2O NWAs/Cu photocathode has a strong photoresponse to the simulated solar light whose photocurrent reaches as much as 0.4 mA cm^{-2}. The short circuit current (J_{SC}) of the PFC composed of TiO_2 NRs/FTO photoanode and C/Cu_2O NWAs/Cu photocathode reaches 0.50 mA cm^{-2} which is more than two times higher than the reported J_{SC} of TiO_2/Ti - Cu_2O/Cu system (0.23 mA cm^{-2}).[21] This value is higher than the sum of the photocurrent of the photoanode and photocathode. It means that the PFC system has a synergistic facilitated effect on the photoresponse of the photoanode and photocathode.

Fig. 1B shows the performance of phenol degradation by photocatalysis with TiO_2 photoelectrode and TiO_2 NRs/FTO - C/Cu_2O NWAs/Cu PFC with or without light illumination, respectively. As we can see from the TOC removal rate of phenol the degradation efficiency of PFC system improve significantly with high TOC removal rate compared with that photocatalyzed by TiO_2 photoanode and Pt system. There is no TOC removal of phenol when no light is illuminated on the TiO_2 NRs/FTO photoanode and C/Cu_2O NWAs/Cu photocathode. Because TiO_2 is a UV-light response semiconductor, there is a weak response to the simulated solar light. So the degradation rate of phenol is very poor, only 6.4%. However, the PFC has a strong response to the solar light due to the existence of C/Cu_2O NWAs/Cu photocathode and the synergistic effect of the two photoelectrodes. So its degradation rate of phenol reaches as much as 84.2 %.The incident photon-to-electron conversion efficiency (IPCE) of the PFC can be calculated by the equation:

$$\mathrm{IPCE}(\%) = \left[1240I/(\lambda J_{light})\right] * 100\% \qquad (1)$$

Where I is the photocurrent density (mA cm^{-2}), J_{light} is the incident irradiance (mW cm^{-2}) and λ is the incident light wavelength. The IPCE curve are shown in Fig. S5.

At the same time, the photocurrent and degradation rate of phenol on different PFCs has been studied. Herein, eight kinds of (8 PFCs) mentioned above have been chosen to study the photocurrent. Table 1 shows that the J_{SC} of TiO_2 NRs/FTO-C/Cu_2O NWAs/Cu PFC reaches as much as 0.50 mA cm^{-2}. The Jsc (TiO_2 NRs/FTO PFC) is higher than Jsc (TiO_2 NTs/Ti PFC) with same photocathode. Because the photoresponse of photoanodes determine the relationship of the two J_{SC} when the phtotcathode is fixed. This could be attributed to the single crystal structure of the TiO_2 NRs/FTO (see in Fig. S2 A3). The PEC performance of the TiO_2 NRs/FTO-C/Cu_2O NWAs/Cu PFC is the best of all. For the PFC with the same photoanode, J_{SC} of C/Cu_2O/Cu is larger than that of Cu_2O/FTO. The reason speculated is not only the photoresponse of the photocatalyst to the solar light but also the conductivity of the substrates.

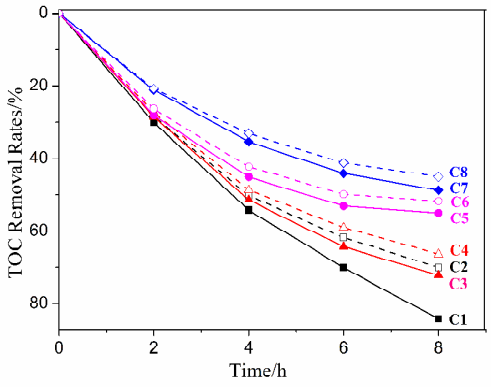

Journal of Materials Chemistry A Accepted Manuscript

Fig. 2 The TOC removal rate of phenol (20 mg L^{-1}) of 8 PFCs using two electrode configuration under AM 1.5 illumination, 0.1 mol L^{-1} Na_2SO_4 as support electrolyte. Here, C1 to C8 is the number of the PFC which is the same with that in Table 1.

These TOC removal rates of phenol on 8 PFCs have been studied. Here the concentration of the phenol is 20 mg L^{-1}, and the support electrolyte is 0.1 mol L^{-1} Na_2SO_4. In Fig 2, the TOC removal rate of phenol on TiO_2 NRs/FTO-C/Cu_2O NWAs/Cu PFC is the highest, which reaches 84.2%. The result is consistent with that of J_{SC} comparison. However, there is an exception. With the same photocathode, the TOC removal rate of phenol of PFC with CdS/FTO photoanode is lower than that of TiO_2 NRs/FTO and TiO_2 NTs/Ti, but the J_{SC} of CdS/FTO photoanode PFC is higher. Because the J_{SC} of the PFC will continuously decay with light illumination (see in Fig. S4) and the J_{SC} in Table 1 is only measured at initial 10 minutes. The J_{SC} of CdS/FTO PFC decays more rapidly due to the serious photocorrosion of CdS. The opposite trend is observed on the J_{SC} of CdS/FTO photoanode is higher than that of TiO_2 NTs/Ti. The J_{SC} of CdS/FTO photoanode decays obviously with time increasing. After 6 hours, the J_{SC} is only tenth of initial photocurrent density. So we can see that there is little effect in the last 2 hours in phenol degradation. In these 8 PFCs, the CdSe/FTO - Cu_2O/FTO PFC has the lowest TOC removal rate of 42% on phenol.[19,20]

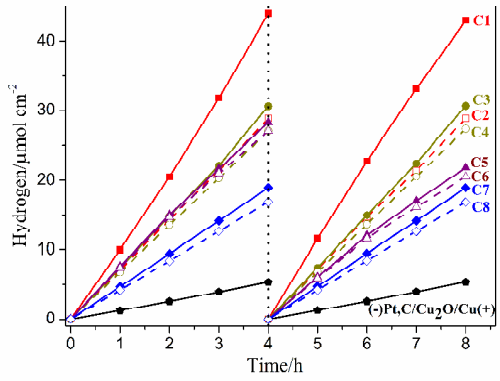

Fig. 3 Hydrogen production of the 8 PFCs and Pt- C/Cu_2O /Cu.

In the hydrogen production experiments, the closed reactor was purged with N_2 to ensure the air-proof conditions, and the gas composition was monitored in the whole cycles. The standard H_2 peak of the GC spectra appears when the retention time is 1.2 min (Fig. S6) and the hydrogen-producing rate in 8 h of 8 PFCs are shown in Fig. 3. The average hydrogen-producing rate of the TiO_2 NRs/FTO-C/Cu_2O NWAs/Cu PFC reaches about 11 μmol $h^{-1}cm^{-2}$(normalized to the cathode area) and for 8 h the total rate is 86.8 μmol cm^{-2} which is the best of all. This result is higher than the hydrogen production by BPEC.[43] For comparison, the hydrogen-producing rate of Pt-C/Cu_2O NWAs/Cu reduces to only 1.4 μmol h^{-1} cm^{-2} and the total is 10.6 μmol cm^{-2}. The result of hydrogen-producing rate of different PFCs is consistent with that of J_{SC}, too. Like with the TOC removal rates, for the CdS/FTO photoanode PFC, the hydrogen-producing rate decreases much in the last 4 h due to the serious photocorrosion of CdS. So the hydrogen-producing rate of it is not the highest. However, when the semiconductor anode is replaced by the Pt, the hydrogen-producing rate has a great decrease. These results also prove that there is a synergistic facilitated effect between the two photoelectrodes of the PFC which is confirmed by the results of TOC removal rates of phenol. In Fig. 4, when the current density is 0.32 mA cm^{-2} the power density reaches the maximum (P_{max}) 0.073 mW/cm^2. Table 2 lists the current–voltage characteristics of 8 PFC systems using phenol (0.05 mol L^{-1}) as substrates and Na_2SO_4 (0.1 mol L^{-1}) as electrolyte. The fill factor (FF) which is an important indicator of output characteristics of the PFC can be calculated based on these parameters by the following equation:

$$FF = P_{max}/J_{SC}V_{oc} \quad (2)$$

Where the P_{max} and $J_{SC}V_{OC}$ represent the real maximum power density and theoretical maximum power density yielded from PFC system, respectively. J_{SC} and V_{OC} are short-circuit current density and open-circuit voltage of PFC system.

Table 2 also summarizes the cell parameter such as V_{OC}, J_{SC}, P_{max} and FF, TOC removal rates and hydrogen-producing rates of all PFCs. The results also proves the hydrogen-producing rate and TOC removal rate of phenol increases with the J_{SC} of PFCs. Here we can see the TiO_2 NRs/FTO-C/Cu_2O NWAs/Cu PFC is the best one and its J_{SC} of 0.50 mA cm^{-2}, TOC removal rates of 84.2%,and hydrogen-producing rates of 86.84μmol cm^{-2} which are much higher than other parallel researches.[20,21]

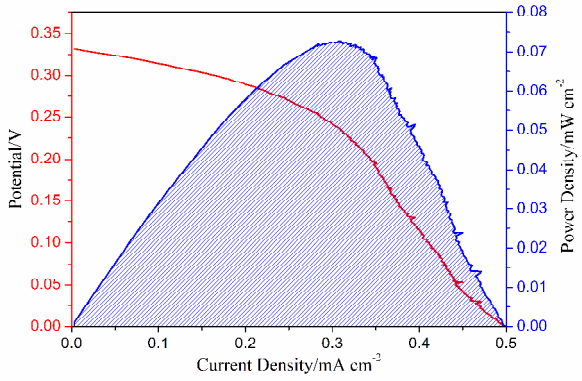

Fig. 4 The I-V characteristic curve (red) and power density curve (blue) of TiO_2 NRs/FTO-C/Cu_2O NWAs/Cu PFC. I-V curves were determined by performing linear sweep voltammetry with a two-electrode system in one typical cycle. The scan rate was 0.02V s^{-1}.

Journal of Materials Chemistry A Accepted Manuscript

Journal Name

RSCPublishing

ARTICLE

Table 2. The photoelectrochemical performance, TOC removal and hydrogen production of PFCs.

No.	PFC Photoanode	PFC Photocathode	V_{OC} (V)	J_{SC} (mA cm^{-2})	P_{max} (mW cm^{-2})	FF	TOC[a] (%)	H_2[b] (μmol cm^{-2})
C1	TiO_2 NRs	C/Cu_2O/Cu	0.41	0.50	0.073	0.36	84.2	86.84
C2	TiO_2 NRs	Cu_2O	0.53	0.25	0.040	0.30	70.1	57.64
C3	TiO_2 NTs/Ti	C/Cu_2O/Cu	0.36	0.33	0.034	0.29	72.2	61.32
C4	TiO_2 NTs/Ti	Cu_2O	0.48	0.20	0.030	0.31	66.4	54.36
C5	CdS	C/Cu_2O/Cu	0.50	0.61	0.092	0.30	55.0	50.05
C6	CdS	Cu_2O	0.62	0.31	0.060	0.31	51.8	47.51
C7	CdSe	C/Cu_2O/Cu	0.27	0.16	0.014	0.32	48.7	37.78
C8	CdSe	Cu_2O	0.39	0.11	0.013	0.30	45.1	33.67

a, TOC is the TOC removal rate of phenol.

b, H_2 is the hydrogen-producing rate.

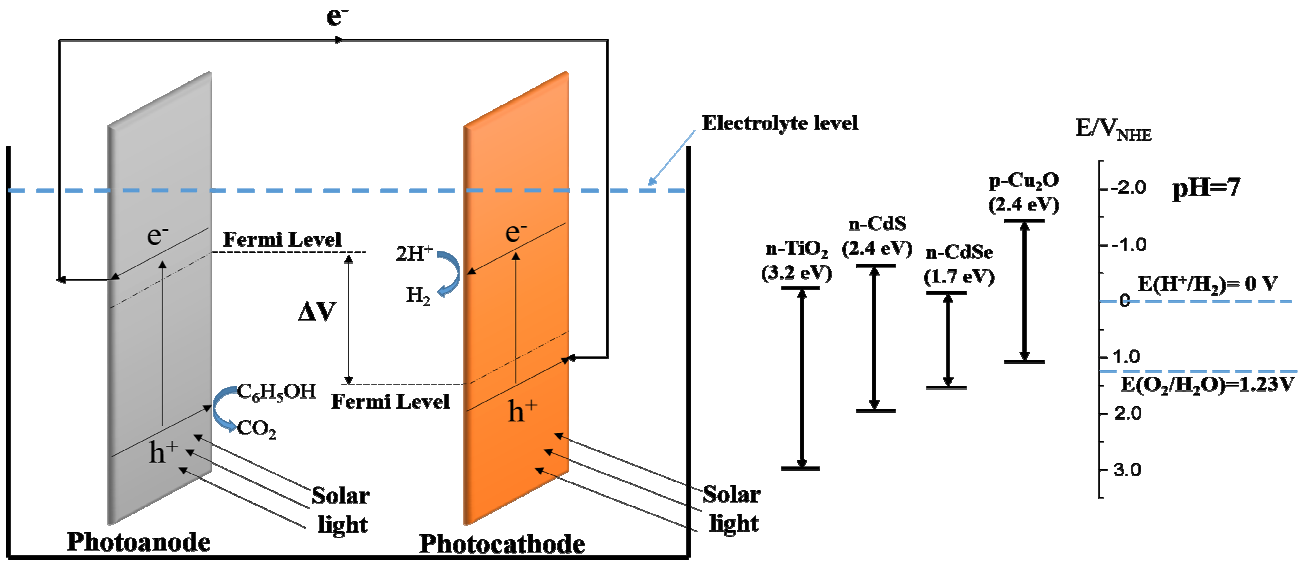

Fig. 5 The working mode diagram of PFC system.

Operation mechanism of dual photoelectrode PFC

The dual photoelectrode PFC is composed of two photocatalytic semiconductor electrodes configuration including n-type semiconductor photoanode and p-type photocathode. Under light illumination, both of the two photoelectrodes can generate electron/hole pairs. The driving force of PFC is the Fermi level difference between the two photoelectrodes. The Fermi level of photoanode should be more negative than that of photocathode, so that a bias will be produced. Then the electrons on the photoanode will transfer through the external circuit to combine with the holes on the photocathode.[20] The holes will be accumulated on the photoanode and electrons at photocathode. So it is a Z-scheme and there is a cooperative synergistic facilitated effect.[44-46] This is why there is a great enhancement of TOC removal rate of phenol and hydrogen-producing rate of PFC compared to the single photoanode (or photocathode) and Pt system. So the PFC can be used for simultaneous pollutants degradation and hydrogen production.

For example, TiO_2 NRs/FTO and C/Cu_2O NWAs/Cu mesh are chosen as the photoanode and photocathode, respectively. The Fermi level of the TiO_2 NRs/FTO photoanode is more negative than that of C/Cu_2O NWAs/Cu mesh photocathode, so in this case a self-driven PFC can be operated under solar light illumination. The remaining holes on TiO_2 NRs/FTO photoanode and electrons on C/Cu_2O NWAs/Cu mesh

Journal of Materials Chemistry A Accepted Manuscript

photocathode can be used for simultaneous organic pollutants degradation and hydrogen production.

Fig. 5 shows the working mode of the PFC. In this PFC, two half-reactions are involved: the organics oxidized by the solar light illuminnation in the anode and water reduction to hydrogen in the cathode. The overall reaction process can be described as the equation (2)-(6):

$$TiO_2 + h\nu \rightarrow h^+_{vb1} + e^-_{cb1} \quad (3)$$

$$C_6H_5OH + 5H_2O + 16h^+_{vb1} \longrightarrow 6CO_2 + 16H^+ \quad (4)$$

$$Cu_2O + h\nu \rightarrow h^+_{vb2} + e^-_{cb2} \quad (5)$$

$$e^-_{cb1} + h^+_{vb2} \longrightarrow h\nu' \quad (6)$$

$$2H^+ + 2e^-_{cb2} \longrightarrow H_2 \quad (7)$$

The photovoltage of TiO_2 NRs/FTO photoanode, C/Cu_2O NWAs/Cu mesh photocathode and the PFC combined by them are measured to confirm this operation mechanism. As shown in Table 3, the photovoltage of TiO_2 NRs/FTO photanode and C/Cu_2O NWAs/Cu mesh photocathode were measured respectively with and without AM 1.5 illumination in the electrolyte of 0.1 mol L^{-1} Na_2SO_4. The TiO_2 NRs/FTO photanode and C/Cu_2O NWAs/Cu mesh photocathode have a quick photoresponse and the voltage value change from -0.08 V to -0.33 V and 0.02 V to 0.18 V instantaneously when the light source is turned on. So the photovoltage of TiO_2 NRs/FTO photanode and C/Cu_2O NWAs/Cu mesh photocathode were 0.25 V and 0.16 V, resectively. Then the theoretical phtovoltage of the PFC could be calculated to be 0.41V which is the sum of the photovoltage value of the TiO_2 NRs/FTO photanode and C/Cu_2O NWAs/Cu mesh photocathode. The experimental photovlotage (V_{OC}) of the PFC system is about 0.41V which matches that obtained by theoretical calculation. This result indicates that the photovoltage of the PFC authentically originated from the

Table 3. The photovoltage of photoelectrodes and PFCs.

PFC No.	PFC Photoanode	PFC Photocathode	V_1[a] (V)	V_2[b] (V)	V_{OC} (V)	$V_{OC}'=V_1+V_2$ (V)
C1	**TiO_2 NRs**	**C/Cu_2O/Cu**	0.25	0.16	0.41	0.41
C2	**TiO_2 NRs**	**Cu_2O**	0.25	0.28	0.53	0.53
C3	**TiO_2 NTs/Ti**	**C/Cu_2O/Cu**	0.20	0.16	0.36	0.36
C4	**TiO_2 NTs/Ti**	**Cu_2O**	0.20	0.28	0.48	0.48
C5	**CdS**	**C/Cu_2O /Cu**	0.34	0.16	0.50	0.50
C6	**CdS**	**Cu_2O**	0.34	0.28	0.62	0.62
C7	**CdSe**	**C/Cu_2O/Cu**	0.11	0.16	0.19	0.27
C8	**CdSe**	**Cu_2O**	0.11	0.28	0.30	0.39

a, V_1 is the photovoltage of photoanode,

b, V_2 is the photovoltage of photocathod

difference between the Fermi levels of the two photoelectrodes. Such a PFC system can work under solar light illuminationwithout other forms of additional energy by mismatching the Fermi levels of the photoelectrodes.

In order to the further study on the influence of Fermi level of the semiconductor photoelectrodes in PFC, several other semiconductors like n-CdS NPS/FTO, n-CdSe NPs/FTO and n-TiO_2 NTs/Ti have been chosen as photoanode. As we know, the Fermi level of the n-type semiconductor is close to the conduction band and that of p-type semiconductor is close to the valence band. So the position of Fermi level can be determined through the position of the conduction band (E_{CB}) and valence band (E_{VB}). Here, the ΔV which is the difference between the E_{CB} of n-type semiconductor and the E_{VB} of p-type semiconductor stands for the difference of Fermi level between two photoelectrodes. Table 4 shows the energy band parameter of several semiconductors. Theoretically, the greater the difference between the E_{CB} of photoanode and E_{VB} of photocathode is, the greater the V_{oc} of the PFC will be. Table 1 lists the difference between the E_{CB} of photoanode and E_{VB} of photocathode of the PFCs. Therefore the V_{OC} of CdS NPS/FTO-C/Cu_2O NWAs/Cu PFC, TiO_2 NRs/FTO-C/Cu_2O NWAs/Cu PFC and CdSe NPS/FTO- C/Cu_2O NWAs/Cu PFC would range in descending sequence: V_{OC}(CdS NPS/FTO - C/Cu_2O NWAs/Cu) > V_{OC}(TiO_2 NRs/FTO - C/Cu_2O NWAs/Cu) > V_{OC}(CdSe NPS/FTO - C/Cu_2O NWAs/Cu).

Table 4. The E_{CB} of photoanode, E_{VB} of photocathode and difference between them of PFCs.[22]

PFC Photocathode	PFC Photoanode	p-E_{VB} (V)	n-E_{CB} (V)	ΔV=(p-E_{VB} - n-E_{CB}) (V)
p-Cu_2O	**n-CdS**	1.10	-0.52	1.39
p-Cu_2O	**n-TiO_2**	1.10	-0.29	1.62
p-Cu_2O	**n-CdSe**	1.10	-0.10	1.20

Here we can see when the photoanode of the PFC is the CdSe/FTO the VOC of the PFC is lower than the sum of photovoltage of photoanode and photocathode while other PFCs equal to the sum. The main reason speculated is the difference of Fermi level between CdSe and Cu_2O is the smallest of all so that the small difference of Fermi level would not maximize the V_{OC} of PFC.

As shown in Table 4, the V_{OC} of CdS NPS/FTO-C/Cu_2O NWAs/Cu has a maximum value of 0.50 V among the three

Journal of Materials Chemistry A Accepted Manuscript

PFCs. And the Voc value of TiO_2 NRs/FTO - C/Cu_2O NWAs/Cu and CdS NPS/FTO-C/Cu_2O NWAs/Cu are 0.41 V and 0.20 V, respectively. They also range in a same descending sequence with theoretical speculation. Therefore, it is reasonable that V_{OC} of the PFC is determined by the difference of Fermi level between the two photoelectrodes. What's more, the V_{OC} value of PFC increases with the difference of Fermi level between the two photoelectrodes.

As we know, the V_{OC} of the PFC are also influenced by many other factors. These factors can be divided into two categories: (1) environmental factors such as temperature, pH value and electrolyte, (2) material factors such as crystal facet and microstructure. While the environmental factors have been studied commonly by so many researchers, the study of material factors is fully discussed here. Therefore, Cu_2O NPs/FTO and TiO_2 NTs/Ti were chosen as the reference photoelectrodes. Table 3 also shows that the V_{OC} value of the PFCs with Cu_2O NPs/FTO photocathode is higher than that of PFCs with C/Cu_2O NWAs/Cu photocathode when their photoanodes are the same. Herein, the key factor that influence the V_{OC} of PFC is the crystal facet structure of the Cu_2O.

In the Fig. 6 A, the XRD pattern of Cu_2O/FTO shows the dominated crystal facet of Cu_2O is (220) which is the high index crystal facet while the dominated crystal facet of C/Cu_2O NWAs/Cu is (111). The (111) has the best photocatalytic ability. Because the high crystal facet (220) has a higher surface energy than the low index crystal facet (111). In a similar way, for the TiO_2 photoanodes with different structure, when the PFCs are composed of the same photocathode, the V_{OC} of the PFC with TiO_2 NRs/FTO is higher than that with TiO_2 NTs/Ti as photoanode. In Fig. 6 B, the dominated crystal facet of TiO_2 NTs/Ti is (101) while that of TiO_2 NRs/FTO is high index crystal facet (002) and (112). Therefore, V_{OC} of TiO_2 NRs/FTO photoanode PFC is higher than that of TiO_2 NTs/Ti photoanode PFC. Here we can see that except for the difference of Fermi level, the microstructure such as crystal facet structure of the photoelectrodes also influence the V_{OC} of PFC. The V_{OC} of PFC increases with the ratio of high index crystal facet of the photoelectrodes.

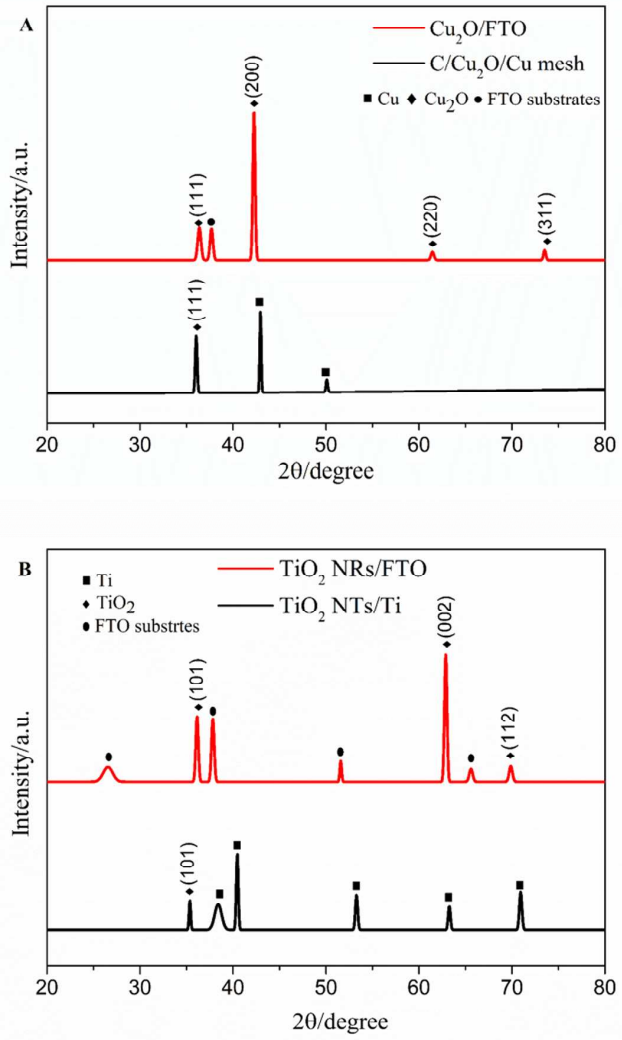

Fig. 6 A: the XRD pattern of Cu_2O NPs/FTO and C/Cu_2O NWAs/Cu; B: the XRD pattern of TiO_2 NRs/FTO and TiO_2 NTs/Ti.

Conclusions

In this work, a dual PFC has been fabricated, which can work without other external energy input except for light illumination. Several n-type and p-type semiconductors have been chosen as the photoanode and photocathode, respectively. The PFC has a superior V_{OC} of 0.41 V and a J_{SC} of 0.50 mA cm^{-2} with TiO_2 NRs/FTO as photoanode and C/Cu_2O NWAs/Cu as photocathode. The best TOC removal rate of phenol and hydrogen production rate in 8 hours reaches 84.2% and 86.8 μmol cm^{-2}, which is much higher than other reported similar studies. For the investigation of mechanism, the V_{OC} value of PFC mainly influenced by the difference of Fermi level between the two photoelectrodes. For the same semiconductors with different microstructure, the crystal facet properties also influence the V_{OC} of PFC. And the V_{OC} value of PFC increases with the ratio of high index crystal facet of photoelectrodes. However the J_{SC} of PFC is not only influenced

Journal of Materials Chemistry A Accepted Manuscript

This journal is © The Royal Society of Chemistry 2014

by the difference of Fermi level between the two photoelectrodes but also by the photoresponse of the photocatalyst and electrical conductivity of the substrate of the photocathode. The higher photocurrent and the better electrical conductivity is displayed, the higher J_{SC} of PFC would be achieved. The tendency of degradation for phenol and hydrogen production are the same with that of J_{SC}. So this work provides a novel and clear theoretical guidance of photoelectrodes selection and exploits a new application of PFC for hydrogen production.

Acknowledgements

This work was supported by the National Natural Science Foundations of China (NSFC, 21477085 and 21277099).

Notes and references

*Corresponding Author: *Phone:* (86)-21-65981180.
Fax: (86)-21-65982287. *E-mail*: g.zhao@mail.tongji.edu.cn
Department of Chemistry, Key Laboratory of Yangtze River Water Environment, Tongji University, Shanghai 200092, People's Republic of China

† Electronic Supplementary Information (ESI) available: the pretreatment of FTO; the detailed preparation procedure of TiO_2 NTs/Ti, CdS/FTO, CdSe/FTO and Cu_2O NPs/FTO; the scheme of quartz reactor; the GC spectra of hydrogen.

1 S. Chu and A. Majumdar, *Nature*, 2012, **488**, 294–303.
2 S. B. Grant, J. D. Saphores, D. L. Feldman, A. J. Hamilton, T. D. Fletcher, P. L. M. Cook, M. Stewardson, B. F. Sanders, L. A. Levin, R. F. Ambrose, A. Deletic, R. Brown, S. C. Jiang, D. Rosso, W. J. Cooper and I. Marusic, *Science*, 2012, **337**, 681–686.
3 M. R, Hoffmann, S. T. Martin, W. Choi and D. W. Bahnemann, *Chem. Rev.*, 1995, **95**, 69-96.
4 B. E. Logan and K. Rabaey, *Science*, 2012, **337**, 686-690.
5 B. E. Logan, B. Hamelers, R. Rozendal, U. Schröder, J. Keller, S. Freguia, P. Aelterman, W. Verstraete, and K. Rabaey, *Environ. Sci. Technol.*, 2006, **40 (17)**, 5181–5192.
6 A. Rinaldi, B. Mecheri, V. Garavaglia, S. Licoccia, P. D. Nardo and E. Traversa, *Energy Environ. Sci.*, 2008, **1**, 417-429.
7 F. Qian, G. Wang and Y. Li, *Nano Lett.*, 2010, **10**, 4686–4691.
8 F. F. Ajayi, K. Y. Kim, K. J. Chae, M. J. Choi, S. Y. Kim, I. S. Chang and I. S. Kim, *Int. J. Hydrogen Energy*, 2009, **34**, 9297–9304.
9 Y. Gao, X. Ding, J. Liu, Lei Wang, Z. Lu, L. Li and L. Sun, *J. Am. Chem. Soc.*, 2013, **135**, 4219−4222.
10 B. Zhang, W. F. Yao, C. P. Huang, Q. J. Xu and Q. Wu, *Int. J. Hydrogen Energy*, 2013, **38**, 7224-7231.
11 A. Paracchino, V. Laporte, K. Sivula, M. Grätzel and E. Thimsen, *Nat. Mater.*, 2011, **10**, 456-461.
12 Q. Li, B. Guo, J. Yu, J. Ran, B. Zhang, H. Yan, and J. R. Gong, *J. Am. Chem. Soc.*, 2011, **133**, 10878–10884.
13 C.Y. Lin, Y. H. Lai, D. Mersch and E. Reisner, *Chem. Sci.*, 2012, **3**, 3482.
14 M. Antoniadou, D. I. Kondarides, D. Labou, S. Neophytides and P. Lianos, *Sol. Energ. Mat. Sol. C.*, 2010, **94**, 592–597.
15 R. L. Chamousis and F. E. Osterloh, *ChemSusChem*, 2012, **5**, 1482–1487.
16 Y. Liu, J. Li, B. Zhou, H. Chen, Z. Wang and W. Cai, *Chem. Commun.*, 2011, **47**, 10314-10316.
17 Y. Liu, J. Li, B. Zhou, S. Lv, X. Li, H. Chen, Q. Chen and W. Cai, *Appl. Catal. B: Environ*, 2012, **111-112**, 485–491
18 B. Wang, H. Zhang, X. Lu, J. Xin and M. K. H. Leung, *Chem. Eng. J.*, 2014, **253**, 174-182.
19 K. Li, Y. Xu, Y. He, C. Yang, Y. Wang and J. Jia, *Environ. Sci. Technol.*, 2013, **47**, 3490−3497.
20 Q. P. Chen, J. H. Li, X. J. Li, K. Huang, B. X. Zhou, W. M. Cai and W. F. Shangguan, *Environ. Sci. Technol.*, 2012, **46**, 11451−11458.
21 J. Y. Li, J. H. Li, Q. P. Chen, J. Bai, B. X. Zhou, *J. Hazard. Mater.*, 2013, **262**, 304-310.
22 M. Grätzel, *Nature*, 2001, **414**, 338-344.
23 B. Kumar, M. Llorente, J. Froehlich, T. Dang, A. Sathrum, C. P. Kubiak, *Annu. Rev. Phys. Chem.*, 2012, 63:541-69.
24 A. Fujishima and K. Honda, *Nature*, 1972, **238**, 37–38.
25 Q. Zheng, B. Zhou, J. Bai, L. Li, Z. Jin, J. Zhang, J. Li, Y. Liu, W. Cai, X. Zhu, *Adv. Mater.*, 2008, **20**, 1044–1049.
26 Y. Ma, X. Wang, Y. Jia, X. Chen, H. Han, and C. Li, *Chem. Rev.*, DOI: 10.1021/cr500008u.
27 A. L. Linsebigler, G. Lu, J. T. Yates, *Chem. Rev.*, 1995, **95 (3)**, 735–758.
28 L. Sang, Y. Zhao and C. Burda, *Chem. Rev.*, DOI: 10.1021/cr400629p.
29 H. J. Zhang, G. H. Chen and D. Bahnemann, *J. Mater. Chem.,* 2009, **19**, 5089–5121.
30 Y. Hou, X. Y. Li, Q. D. Zhao, G. H. Chen and C. L. Raston, *Environ. Sci. Technol.*, 2012, **46**, 4042–4050.
31 M. Wang, L. Sun, Z. Lin, J. Cai, K. Xie and C. Lin, *Energy Environ. Sci.*, 2013, **6**, 1211-1220.
32 W. C. Huang, L. M. Lyu, Y. C. Yang and M. H. Huang, *J. Am. Chem. Soc.*, 2012, **134 (2)**, 1261–1267.
33 E. M. Zahran, N. M. Bedford, M. A. Nguyen, Y. J. Chang, B. S. Guiton, R. R. Naik, L. G. Bachas and M. R. Knecht, J. Am. Chem. Soc., 2014, **136 (1)**, 32–35.
34 P. D. Tran, L. H. Wong, J. Barber and J. S. C. Loo, *Energy Environ. Sci.*, 2012, **5**, 5902-5918.
35 S. Song, Z. Liu, Z. He, A. Zhang and J. Chen, Y. Yang and X. Xu, *Environ. Sci. Technol.*, 2010, **44 (10)**, 3913–3918.
36 R. Vinu and G. Madras, *Environ. Sci. Technol.*, 2008, **42 (3)**, 913–919.
37 J. H. Bang and P. V. Kamat, *Adv. Funct. Mater.*, 2010, **20**,1970–1976.
38 S. N. Chai, G. H. Zhao, Y. N. Zhang, Y. J. Wang, F. Q. Nong, M. F. Li and D. M. Li, *Environ. Sci. Technol.*, 2012, **46 (18)**, 10182–10190.
39 L. F. Fan, G. H. Zhao, H. J. Shi, M. C. Liu, Y. A. Wang, and H. Y. Ke, *Environ. Sci. Technol.*, 2014, **48 (10)**, 5754–5761.
40 S. Banerjee, S. K. Mohapatra, P. P. Das and M. Misra, *Chem. Mater.*, 2008, **20**, 6784–6791.
41 Z. Zhang, R. Dua, L. Zhang, H. Zhu, H. Zhang and P. Wang, *ACS Nano*, 2013, **7**, 1709-1717.
42 Q. T. Du, J. S. Tan, Q. T. Wang, C. Y. Li, X. H. Liu, R. S. Cai, Y. H. Ding, and Y. Q. Wang, *J. Anal. Methods. Chem.*, 2012, **406162**, 1-8.

Journal of Materials Chemistry A Accepted Manuscript

43 G. L. Zang, G. P. Sheng, C. Shi, Y. K. Wang, W. W. Li and H. Q. Yu, *Energy Environ. Sci.*, 2014, **7**, 3033-3039.
44 H. Tada, T. Mitsui, T. Kiyonaga, T. Akita and K. Tanaka, *Nat. Mater.*, 2006, **5**, 782-786.
45 K. Maeda, *ACS Catal*. 2013, **3**, 1486 −1503.
46 P. Zhou , J. Yu and M. Jaroniec, *Adv. Mater.*, 2014, **26**, 4920–4935.

Journal of Materials Chemistry A Accepted Manuscript

 This journal is © The Royal Society of Chemistry 2014